AIAA JOURNAL
Vol. 32, No. 5, May 1994

Reattachment Studies of an Oscillating Airfoil Dynamic Stall Flowfield

S. Ahmed*
MCAT Institute, San Jose, California 95127
and
M. S. Chandrasekhara†
Naval Postgraduate School, Monterey, California 93943

The reattaching flow over an oscillating airfoil executing large-amplitude sinusoidal motion around a mean angle of attack of 10 deg has been studied using the techniques of stroboscopic schlieren, two-component laser Doppler velocimetry, and point diffraction interferometry, for a freestream Mach number of 0.3 and a reduced frequency of 0.05. The results show that the dynamically stalled flow reattaches in a process that begins when the airfoil is very close to the static stall angle on its downward stroke and progresses over the airfoil through a large range of angles of attack as the airfoil angle decreases to about 6 deg. The airfoil suction peak shows a dramatic rise as the static stall angle is approached, and the velocity profiles develop such that the flow near the surface is accelerated. The process completes through the disappearance of a separation bubble that forms over the airfoil.

Nomenclature

C_p = pressure coefficient
$C_{p\max}$ = maximum pressure coefficient
c = airfoil chord
f = frequency of oscillation, Hz
k = reduced frequency, $\pi fc/U_\infty$
M = freestream Mach number
U, V = velocity components in the x and y directions
U_∞ = freestream velocity
$\mathcal{V}$ = total velocity, $\sqrt{U^2 + V^2}$
x, y = chordwise and vertical distance
α = angle of attack
α_m = amplitude of oscillation
α_0 = mean angle of attack
γ = ratio of specific heats
ε = fringe number
ρ = density
ρ_r = density at reference conditions
ϕ = phase angle of oscillation
ω = circular frequency, rad/s

I. Introduction

FLOWS over oscillating airfoils have received considerable attention as the need to improve the performance of a helicopter has increased. The performance limitation stems from the leading-edge flow separation causing dynamic stall[1] on the retreating blade of a helicopter during the pitchup stroke. The flow eventually reattaches later in the pitchdown cycle. Depending on the mean angle of attack, amplitude, and frequency of oscillations, a hysteresis loop of varying size develops.[2] It is known that the hysteresis loop determines the aerodynamic damping. Whereas extensive studies have been carried out on oscillating airfoils to understand the dynamic stall process, the reattachment of the unsteady separated flows has received little attention. Reattachment of unsteady separated flows is a topic of basic research in itself, since several issues of flow separation and attachment are involved, such as the local pressure gradient, the state of the separated shear layer, its ability to overcome the adverse pressure gradient, and so on. An understanding of the process may also help in modifying the flow. For example, if the process can be completed rapidly, the airfoil can generate more lift through the cycle, thus altering its performance. The changes in the pressure distribution that occur over the airfoil may for some conditions cause limit cycle oscillation. A parameter based on the pitching moment of the airfoil (which in turn is dictated by the hysteresis loop) was defined[2] to determine the aerodynamic damping over the cycle of oscillation. It was observed that the damping could become negative during certain parts of the cycle, resulting in an increase in the amplitude of oscillations leading to stall flutter. An understanding of the reattachment process is therefore essential to alleviate the stall flutter and to improve the dynamic lift characteristics of an oscillating airfoil.

Niven et al.[3] made the first attempt to analyze the reattachment of separated flow of a two-dimensional wing undergoing ramp-down motion through surface pressure measurements. This study showed that the reattachment process occurs over a finite length of time and the airfoil incidence at reattachment was found to be close to the static stall angle. However, no flowfield measurements were available to understand the physics involved in the process. The present study at the Navy-NASA Joint Institute of Aeronautics being conducted in the NASA Ames Research Center, Fluids Mechanics Laboratory (FML), is aimed at understanding the mechanisms involved in the separation and reattachment of flows associated with oscillating airfoils through flowfield analysis using a variety of experimental techniques. The experimental techniques used included the schlieren method for qualitative analysis of the global flowfield, laser Doppler velocimetry (LDV) for quantitative measurements of the velocity field, and point diffraction interferometry (PDI) for measurements of density and pressure distributions. The initial studies of the dynamic stall problem were confined to the upstroke of the oscillation cycle to understand the mechanism of separation leading to the dynamic stall and the effects of compressibility on dynamic stall. Results of schlieren studies by Chandrasekhara and Carr[4] on an oscillating airfoil have indicated that compressibility effects set in at $M = 0.3$. Further studies by Chandrasekhara and Ahmed[5] using LDV have shown the formation of a separation bubble near the leading edge before the formation of a dynamic stall vortex. Studies with the PDI technique by Carr et al.[6,7] have confirmed the presence of a separation

Presented as Paper 91-3225 at the AIAA 9th Applied Aerodynamics Conference, Baltimore, MD, Sept. 23–25, 1991; received Jan. 14, 1992; revision received Oct. 8, 1993; accepted for publication Oct. 19, 1993.

*Research Scientist; on leave from National Aeronautical Laboratory, Bangalore, India. Member AIAA.

†Research Associate Professor and Associate Director, Navy-NASA Joint Institute of Aeronautics, Department of Aeronautics and Astronautics; Mailing address: M.S. 260-1, NASA Ames Research Center, Moffett Field, CA 94035. Associate Fellow AIAA.

bubble and shown that the flow gradients are slower to develop in the oscillatory case compared with the steady state resulting in the delay of stall known as dynamic stall.

In this paper, results obtained on an oscillating NACA 0012 airfoil as it executes the downward stroke are presented. Flowfield data obtained using three different experimental techniques are discussed, and an attempt is made to describe the reattachment process of the separated flowfield.

II. Description of the Experiment

A. Facility

The experiments were conducted in the FML Compressible Dynamic Stall Facility (CDSF). The CDSF is an indraft wind tunnel with a 35 × 25 cm test section. The oscillatory motion is produced by a drive system located on top of the test section. It is connected to the test section windows by connecting rods on either side. The windows are mounted in bearings, and the airfoil is supported between the windows by pins that are smaller than the local airfoil thickness. This enables optical access down to the airfoil surface. A sinusoidal motion of the windows results in a sinusoidal variation of the airfoil angle of attack.

The drive is equipped with incremental position encoders that provide the airfoil instantaneous angle of attack and frequency/phase angle of oscillation. An absolute position encoder indicates the angle of attack. The specifications of the tunnel and drive system are

$$\alpha = \alpha_0 + \alpha_m \sin 2\pi\, \text{ft} = \alpha_0 + \alpha_m \sin \omega t$$

$$0 \le \alpha_0 \le 15 \text{ deg}$$

$$2 \le \alpha_m \le 10 \text{ deg}$$

$$0 \le f \le 100 \text{ Hz}$$

$$0 \le M \le 0.5$$

$$2 \times 10^5 \le Re \le 10^6$$

$$\text{airfoil chord} = 7.62 \text{ cm}$$

The airfoil angle, reduced frequency, and Mach number correspond to those of a helicopter in forward flight, and the Reynolds number corresponds to that of a one-seventh scale model rotor, whose test results are directly applicable to a helicopter rotor.

The tunnel is connected to a 240,000-cfm, 9000-hp evacuation compressor that allows continuous running at all flow speeds. Other details of the system can be found in Carr and Chandrasekhara.[8]

B. Measurement Techniques

Three different nonintrusive optical diagnostic techniques were used in the study. These were 1) stroboscopic schlieren, 2) two-component, frequency-shifted, and phase-averaged LDV, and 3) stroboscopic PDI. These are briefly described next.

1. Stroboscopic Schlieren Studies

A standard 3-m focal length, mirror-based schlieren system was set up in a "Z" type configuration with a xenon arc lamp light source at the focal length of one of the mirrors. The beam passing through the test section was focused on a vertical knife edge and then directed to imaging optics. The light source was triggered externally at the desired phase angles by an electronic circuit that compared the chosen phase angle of oscillation and the encoder data from the drive system and produced a TTL pulse when a match occurred. No delays were found to be present between the events of matching the phase angle and light flashing.

2. Unsteady Flow LDV Studies

A two-color, two-component, frequency-shifted argon-ion laser-based TSI system was used for velocity measurements. The system was operated 15 deg off axis, in the forward scatter mode. Traversing was accomplished by directing the four beams onto a 352-mm focal length lens mounted on a computer-controlled traverse. The signals were processed by TSI 1990 counters.

Special phase-locking circuitry was built for handling the random LDV data and the unsteady position data. This was used as an integral part of the data acquisition instrumentation. The LDV data were acquired in the coincidence mode with the coincidence window width arbitrarily set to 50 μs. The coincidence pulse was used to trigger data acquisition and also to freeze the rapidly changing encoder output until the data transfer to the computer could be completed. The software for data acquisition and processing included the standard tests of data validation, phase averaging by binning the data appropriately, identifying gaps in the data if the number of samples in any bin was less than a preselected value (50 in this case), and providing phase distributions of the velocity components. Any time the standard validation criteria were not satisfied, the data set was rejected and new data were acquired. Seeding was accomplished by injecting 1-μm polystyrene latex particles suspended in alcohol into the tunnel inlet. A minimum of 10,000 samples were collected per channel at each measurement point. The complete details of the scheme can be found in Chandrasekhara and Ahmed.[5]

3. PDI studies

PDI is a real-time interferometry technique that uses fluid density changes to produce flow interferograms. Figure 1 shows the schematic of the optical arrangement used. It is similar to a standard schlieren system, with the light source replaced by a pulsed Nd-YAG laser and a predeveloped photographic plate located at the knife edge plane. The principle has been detailed in Refs. 6 and 7 and is only briefly described here. A pinhole was created (burned) in situ in the photographic plate by increasing the laser energy, with no flow in the wind tunnel. This served as the point diffraction source for producing spherical reference waves. When the flow was turned on, the cylinder of light passing through the test section experienced phase shifts depending on the local flow conditions and the beam exiting the tunnel window focused to a slightly larger spot around the pinhole. Since light passing through the pinhole loses all the phase information introduced by the flow due to the spatial filtering characteristics of the pinhole, a reference wave is created in the light beam passing beyond the pinhole. This reference wave subsequently interfered with light that was transmitted around the pinhole through the photographic plate, producing interference fringes in real time at the image plane of the optics system. Reference 9 describes the full details of the actual implementation of the technique in the CDSF. In operation, the laser was triggered stroboscopically, in a manner similar to that used in the schlieren studies. A pulse generated by a photodiode that responded to the actual laser light flash was used to freeze the encoder display, so that the actual phase angle at which an interferogram was obtained could be recorded.

C. Experimental Conditions

The flow Mach number was set to 0.3; the corresponding Reynolds number was 5.4×10^5. The oscillation frequency was 21.6 Hz, which corresponded to a reduced frequency of 0.05. The airfoil was oscillated about the 25% chord point, with its angle of attack varying as $\alpha = 10 \text{ deg} - 10 \text{ deg} \sin \omega t$. The LDV probe vol-

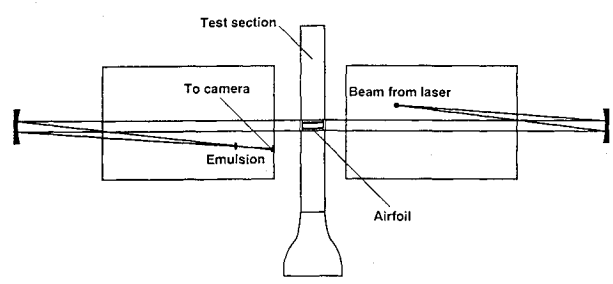

Fig. 1 Schematic of optics layout for point diffraction interferometry.

ume was traversed in the range $-0.25 \leq x/c \leq 0.75$ and $0.0 \leq y/c \leq 0.58$. The data to be presented and discussed will pertain to the downstroke and envelope angles of attack from 15.9 to 0 deg. As stated in Sec. II.A, the conditions chosen correspond to those of a one-seventh scale model rotor whose test results are directly applicable to those of a helicopter.

III. Results and Discussion

The results are discussed in three parts. The first part contains flow visualization pictures obtained using the schlieren technique; the second part presents the LDV data in the reattaching phase of the flow; the results of the PDI studies are discussed in the last part.

A. Schlieren Studies

1. Steady Flow Behavior

Figure 2 shows schlieren pictures of steady attached and separated flowfields on the NACA 0012 airfoil at $M = 0.3$. Figure 2a was obtained for $\alpha = 12.33$ deg, and it is clear that the flow is completely attached. (The two streaks in the figure at the 70% chord location are cracks in the glass window supporting the airfoil. The slight bulge seen at the 50% chord location are 0.15-mm cushions used to prevent direct contact between the metal airfoil and the glass windows.) In the picture, the dark region near the leading edge on the lower side represents the flow at the stagnation point. The white region following it shows density gradients due to acceleration of the flow through the suction peak. The dark patch after this is the region where a laminar separation bubble forms.[7] At high angles of attack, the boundary layer thickens considerably near the trailing edge, as can be seen in the figure. At one encoder count higher, $\alpha = 12.41$ deg, the flow separates, and this state is shown in Fig. 2b. The flow could be brought back to the attached state by simply returning to the lower angle of attack of 12.33 deg, demonstrating the very small hysteresis that was present in steady flow. The two pictures clearly demonstrate the abruptness of flow separation and reattachment in steady flow.

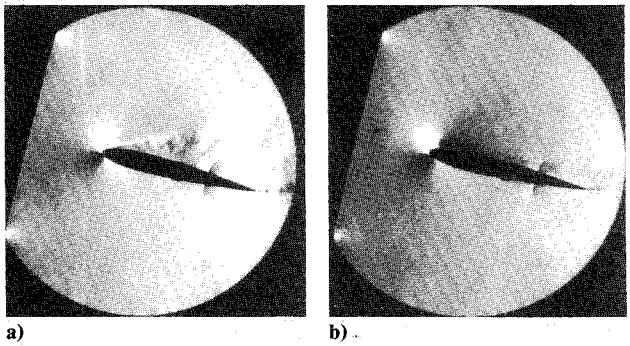

Fig. 2 Schlieren photographs of steady flow behavior near stall: a) α = 12.33 deg and b) α = 12.41 deg.

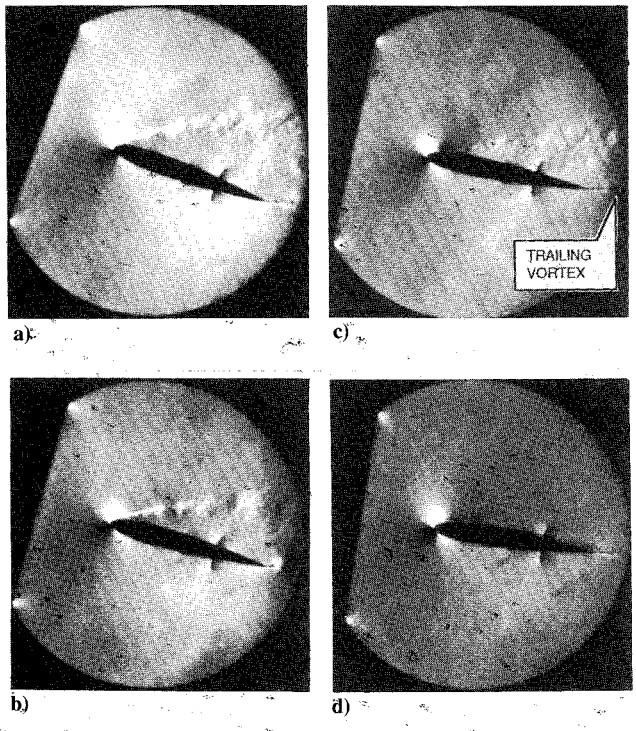

Fig. 3 Schlieren photographs of reattachment process: a) α = 20.0 deg, b) α = 13.82 deg, c) α = 10.0 deg, and d) α = 6.17 deg.

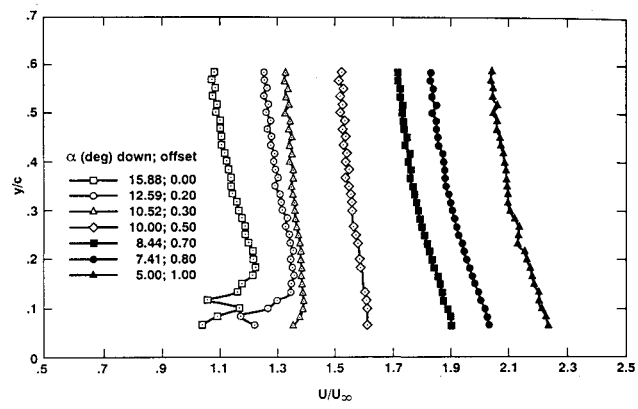

Fig. 4 Distributions of streamwise velocity component U during reattachment; x/c = 0.25 (velocity offset by amounts shown).

2. Unsteady Flow Behavior

Contrary to steady flow, reattachment in unsteady flows is a process occurring over a range of angles of attack (time). Figure 3 presents stroboscopic schlieren pictures as the airfoil executes the downstroke sinusoidally from $\alpha = 20$ to 0 deg. At $\alpha = 20$ deg, the flow is completely separated from the leading edge as seen in Fig. 3a. The flow features to be noted are the stagnation point, the separated shear layer emanating from the airfoil leading edge, and the trailing edge shear layer. The organized vortical structures seen in Figs. 3a and 3c are believed to have originated from the instabilities in the separated shear layer. It is unclear whether these vortices play any role in the reattachment process. For $\alpha = 13.82$ deg, in Fig. 3b, the flow has begun to reattach around the leading edge, but over most of the upper surface, it is still separated. A trailing vortex can be seen in the wake at about 10–15% chord distance from the trailing edge, which is the starting vortex related to partial reattachment. This suggests that the airfoil has already begun to generate lift. At $\alpha = 10$ deg, Fig. 3c, the reattachment has progressed to about 10% chord from the leading edge. A trailing vortex is also present. But the significant point of interest is the appearance of a dark region near the leading edge in the reattached flow. A dark region in the schlieren image represents deceleration for the knife edge orientation used in the present experiment. Hence, on either side of this region, the flow is accelerating. It is believed that a separation bubble forms in this region, in which the leading-edge boundary layer separates and then reattaches. Studies by Carr et al.[7] have shown that a bubble forms during the upstroke of the airfoil and is still present at $\alpha = 10$ deg. It is interesting to note that, even during the downstroke, a similar feature is present (see also Sec. III.C). Figure 3d presents the result for $\alpha = 6.1$ deg, and it is clear that the flow has reattached over the entire airfoil. However, a slight imprint of the separation bubble can still be observed at $x/c \simeq 0.1$ as the flow is accelerating on either side of this point. It was found that only for $\alpha < 6$ deg the separation bubble was not present. This confirms that flow reattachment after dynamic stall is a process taking place over a large range of angles of attack, $12.4 \geq \alpha \geq 6$ deg. Whereas the flow on the upstroke was attached for all of these angles of attack, at corresponding angles of attack on the downstroke, the flow was still separated, indicating the presence of strong hysteresis effects in the flow.

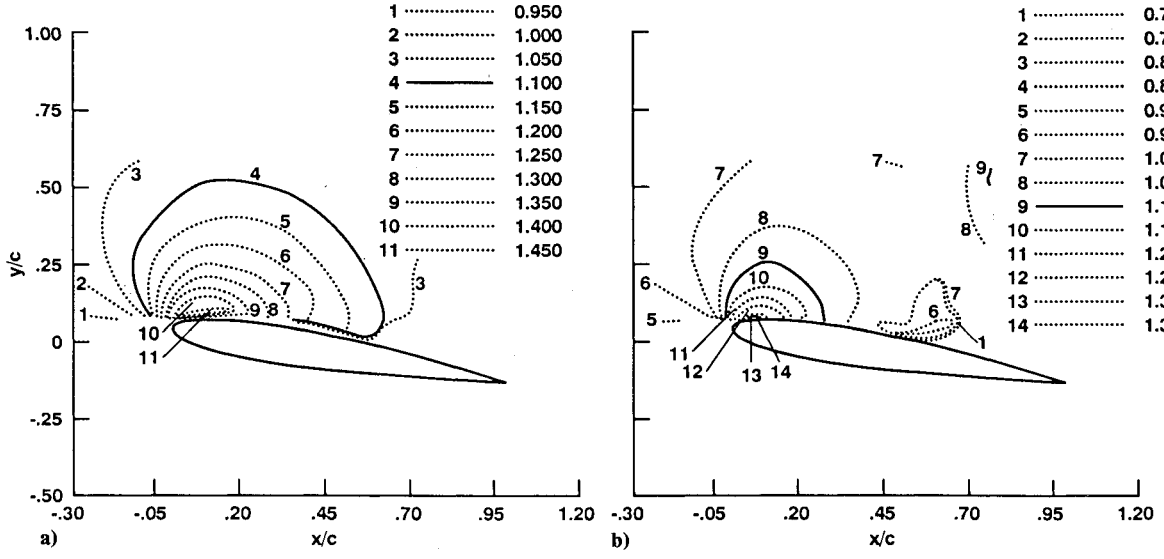

Fig. 5 Contours of total velocity $\mathcal{V}$ at $\alpha = 10.0$ deg: a) upstroke and b) downstroke.

B. LDV Studies

As stated in Sec. II.C, the LDV measurements were carried out over $-0.25 \leq x/c \leq 0.75$ and $0.0 \leq y/c \leq 0.58$. Typical results derived from these measurements are discussed next. Because of limited space, only selected data are presented.

1. Progression of the Reattachment Process

Figure 4 shows profiles of the streamwise velocity component U, for $x/c = 0.25$ at different angles of attack, from $\alpha = 15.88$ deg when the flow is separated to when full reattachment occurs. A defect can be seen in the velocity profiles closer to the airfoil for $0.067 \leq y/c \leq 0.2$ in it. The defect is large ($\simeq 0.3U_\infty$) and extends over a large height above the airfoil surface at an angle of attack of $\alpha = 15.88$ deg. But, at lower angles, it decreases. At $\alpha = 10.52$ deg, the velocity profile becomes smooth with decreasing values toward the surface. However, at $\alpha = 8.44$ deg, the distribution shows increasing velocity near the surface. In the dynamic stall flow, it has been found[5] that the fluid close to the airfoil surface in attached flow is accelerated to values considerably higher than the freestream velocity. Hence, the larger values indicate that the reattachment has progressed to this location. Further decrease in the angle of attack to $\alpha = 7.41$ deg results in the establishment of a flow where the local velocities near the surface increase above the freestream value. Thus, during the reattachment process, the velocity profiles over the airfoil change from those with a defect to those in which the fluid is increasingly accelerated as the surface is approached through the process. Data at other x/c locations confirmed this observation.

2. Comparison of Velocity Distributions on the Up- and Downstroke

A comparison of the total velocity $\mathcal{V}$ on the upper surface at $\alpha = 10$ deg on the upstroke and downstroke is made in Figs. 5a and 5b. The peak velocity reached is about $1.45\ U_\infty$ during the upstroke, whereas during the downstroke it is $1.35\ U_\infty$. Also, the velocity data for the downstroke show low velocities on the order of $0.7U_\infty$ beyond 30% chord, and the extent of, for example, $\mathcal{V} = 1.1U_\infty$ (the solid line in the figure) is nearly half that during the upstroke. Some of the differences between the upstroke and downstroke occur because of the hysteresis effects (due to the large-scale flow separation). At $\alpha = 10$ deg, the flow is partially attached on the downstroke and fully attached on the upstroke. Thus, the changes seen could also be attributed to the pressure effects induced by the moving airfoil. This implies that the pressure distribution over the airfoil is also significantly modified at the same angle of attack, a factor that needs to be included in any calculations of the flow if the forces and moments through the cycle are to be satisfactorily computed.

It was found that the velocity profiles agreed on the two strokes at angles of attack below 5.46 deg, indicating that the hysteresis effects are present for a while longer after reattachment is complete.

C. PDI Studies

1. Interpretation of Interferograms

The interferogram fringes in an aerodynamic flow are contours of constant density. The quantitative nature of the interferograms enables computation of the pressure distribution over the airfoil when the flow is attached, using isentropic flow relations. In the present study, this assumption is made for the boundary-layer fringes also. It is believed that the changes due to the vortical nature of the flow in a thin boundary layer do not significantly affect the nature of the distributions. The density along any fringe can be calculated from the Gladstone-Dale equation[10] for the present wind tunnel and laser used as

$$\rho - \rho_r = 0.009421\varepsilon$$

where the fringe number ε is $0, \pm1, \pm2, \ldots$, for the bright fringes and $\pm1/2, \pm3/2, \pm5/2, \ldots$, for the dark fringes. Fringes from the freestream to the stagnation point have positive values. Hence, by simply counting the fringes from the stagnation point, the fluid density along any fringe can be determined. The corresponding C_p distributions can be computed from the relation

$$C_p = \frac{\left[(\rho/\rho_r)^\gamma - 1\right]}{\left[(\gamma/2)M^2\right]}$$

Knowing the density values, one can determine the corresponding local Mach number.

The triangular pointers seen in the interferograms are registration markers used for scaling and obtaining the pressure distributions. The line joining the vertical edges of the right markers passes through $x/c = 0.25$. The vertical side of the left marker is at $x/c = 0.05$.

2. Interferograms of the Reattachment Process

Representative interferograms of the reattaching flow during the downward motion of the airfoil are shown in Fig. 6. Flow stagnation is indicated by the point on the airfoil lower surface near the leading edge where all fringes can be seen to converge. In some figures, the stagnation point appears to be a region because each fringe has a finite width. The fringes in the shear layer show that

the flow has separated from the leading edge. The white and black patches seen between the separated shear layer and the airfoil surface in Fig. 6a at $\alpha = 12.27$ deg indicate pockets of constant density fluid. Separation at this angle of attack occurs from very near the leading edge. It is clear that the velocity variation in the shear layer corresponds to that over the two dark fringes in it, which is about $0.15U_\infty$ (as determined by fringe counting) for the present experiment. In Fig. 6b, at $\alpha = 10.69$ deg, the flow has partially reattached. One of the dark fringes in the shear layer, after following the acceleration around the leading edge, has turned down toward the airfoil and merged with the local boundary layer. However, by $x/c = 0.2$, the fringe once again lifts off from the surface, indicating separated flow from there on. By this stage, a few more fringes appear around the leading edge, indicating further establishment of the flow there.

As the angle of attack decreases to 9.84 deg, in Fig. 6c, the flow reattachment has progressed to about 35% chord, beyond which it is still separated. At the same time the fringe pattern on the upper surface around the leading edge shows that all outer fringes are smoothly shaped, but those closer to the airfoil (between $x/c = 0.02$–0.1), after coming out radially, become nearly parallel to the upper surface and drop vertically before merging with the boundary layer. This is due to the formation of a laminar separation bubble, an event that was found to occur during the upward stroke as well.[7] This can also be seen from Fig. 6b, but it is less definitive. However, the pressure distributions (see the next section) in fact indicate that a bubble is present at $\alpha = 10.69$ deg also. The bubble is still present at $\alpha = 8.01$, Fig. 6d.

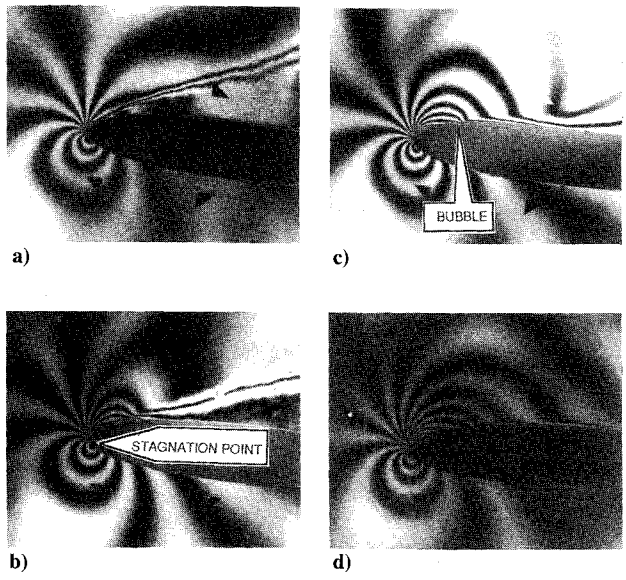

Fig. 6 Interferograms of reattachment process; M = 0.3, k = 0.05, and $\alpha = 10$ deg–10 deg sin ωt: a) $\alpha = 12.27$ deg, b) $\alpha = 10.69$ deg, c) $\alpha = 9.84$ deg, and d) $\alpha = 8.01$ deg.

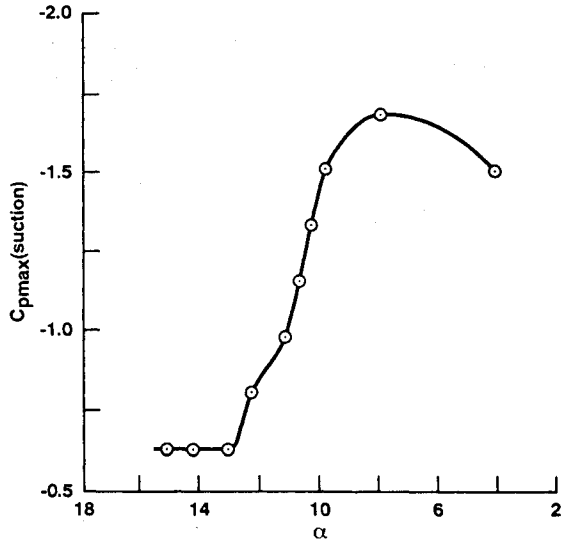

Fig. 7 Variation of maximum suction pressure coefficient.

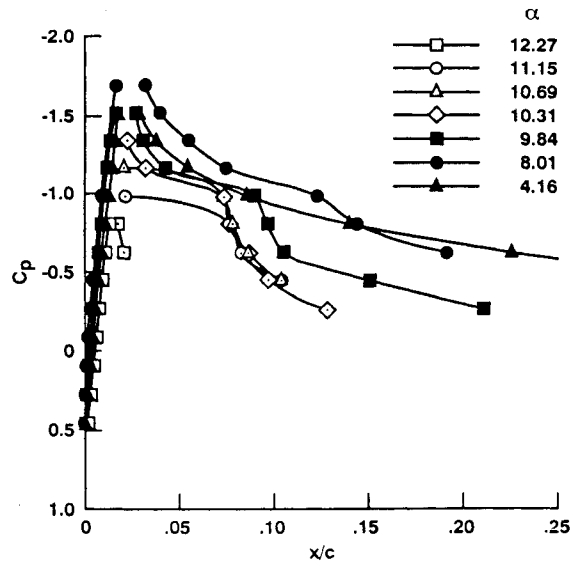

Fig. 8 Pressure distributions during reattachment process.

It is interesting to note that on the upstroke the bubble forms at an angle of attack greater than 5 deg and remains on the surface until the dynamic stall vortex forms at around the static stall angle.[7] The overall flow is still attached until dynamic stall occurs at $\alpha = 15.9$ deg. However, on the downstroke, the flow is partially separated, and the bubble is present only at certain lower angles of attack, $\alpha < 12$ deg. This once again demonstrates the hysteresis effects of the large-amplitude oscillation of the airfoil.

3. *Pressure Distributions During Reattachment*

The variation of the maximum suction pressure coefficient as a function of angle of attack on the NACA 0012 airfoil during the downstroke is plotted in Fig. 7. It shows that as reattachment progresses, the airfoil redevelops suction steadily, during a decrease in angle of attack until $\alpha = 8$ deg. Once the flow has fully established around the airfoil, the suction peak drops with a further decrease of angle of attack as can be expected. Of particular interest and importance is the initial steep increase in the peak suction level at $\alpha \approx 12.6$ deg. It should be noted that this airfoil stalls at $\alpha = 12.41$ deg, at $M = 0.3$ in steady flow (see Sec. III.A). The flow gradients seem to adjust such that as the static stall angle is approached during the downstroke, the leading-edge shear layer begins to reattach, and then flow reattachment begins. A similar observation has also been made by Niven et al.[3] in their study of the reattachment process during rampdown tests on dynamic stall at various pitch rates. The details of the pressure distribution can now be studied to see the salient features of the reattachment process.

Figure 8 presents the pressure distributions at various angles of attack during the downstroke. For $\alpha = 12.27$ deg, only a few fringes could be counted in the accelerating region (up to $x/c = 0.017$ until flow separation); the graph shows that the local $dC_p/dx \approx 500$. For $\alpha = 11.15$ deg, fringes were present in the adverse pressure gradient region beyond $x/c = 0.02$ as well. In between, however, the fringes could not be detected clearly. It can be seen that the suction peak C_p decreases to -1.0, and then a pressure plateau forms until $x/c = 0.083$, after which the pressure increases steeply. Such a behavior is indicative of the presence of a separation bubble, in which a constant pressure region followed by pressure recovery exists. The length of the bubble cannot be determined exactly since its edges could extend beyond this point of increasing pressure as has been pointed out by Tani.[11] The precise determination of its size requires quantification of the stall behavior by

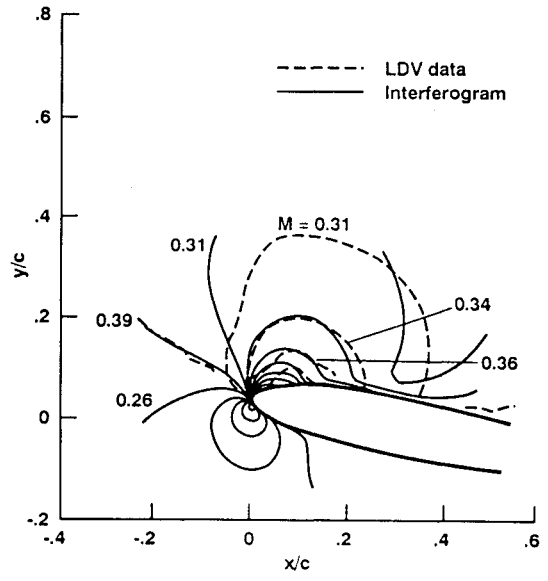

Fig. 9 Comparison of LDV and interferogram data, α = 10.0 deg (downstroke).

other surface flow measurement techniques. It appears that for α = 10.69 and 10.31 deg there is little change in the distributions through the bubble, although the suction peak seems to increase. As the angle of attack decreases, the bubble grows as the boundary layer reattaches further downstream of the leading edge as evidenced by the wider extent of the plateau, for example, at α = 9.84 deg. At the same time, $C_{p_{max}}$ also decreases as flow development continues around the leading edge. At α = 8.01 deg, kinks are still present in the C_p distribution up to x/c = 0.13. Thus, it is possible that a separation bubble is still present even after this location. However, at α = 4.16 deg, the distribution is smooth, and the bubble has disappeared. The peak C_p estimated from these interferograms was −1.7, but the actual $C_{p_{max}}$ is expected to be slightly lower (due to the difficulty of resolving the fringes in this region), whereas the $C_{p_{max}}$ for attached flow on the upstroke is −1.43, and it is −2.12 for steady flow, at α = 4.25 deg. This supports the conclusion that reattachment is a quantitatively different process from the separating flow on the upstroke, even though qualitative similarity exists with regard to the formation of the bubble. In addition, the actual angles of attack at which the various events occur—such as occurrence of the maximum suction peak in the flow, bubble formation, etc.—are different during the upstroke and downstroke due to hysteresis effects that are always present in these unsteady flows.

4. Comparison of LDV and PDI studies

Since two different quantitative measurement techniques were used in the present study, it is instructive to make a direct comparison of the methods and the results obtained. PDI provides a spanwise-averaged instantaneous quantitative flowfield picture, whereas LDV yields a long time-averaged point measurement of the flow. The Mach numbers derived from both methods are compared in Fig. 9 at α = 10 deg, when the airfoil is undergoing downward motion. The solid lines shown in it are the Mach contours corresponding to the centerline of the dark fringes in the interferograms, and the dashed lines are the Mach number contours obtained from LDV (plotted for the corresponding fringe numbers). The agreement is good, considering the vastly different nature of the techniques. The cylinder of light used in PDI provides more data points closer to the airfoil surface, which was not possible with LDV because of the blockage of the beams by the oscillating airfoil. However, the agreement for those data that are coincident demonstrates the statistically stationary nature of even the partially separated flowfield in the region compared. It should be noted that major differences could appear in separated flow regions or in three-dimensional flows.

Since LDV is a point measurement whose resolution is controllable, very detailed surveys of the flow could be obtained. The resolution of PDI is limited to the number of fringes that naturally form based on the laser wavelength, the wind-tunnel span, and the flow density changes. But PDI offers flowfield information instantaneously; obtaining this information would be a very time-consuming task with LDV, a major consideration in high-speed, forced, unsteady flows. The agreement obtained in this study enhances the confidence level of the results presented.

D. Picture of the Reattachment Process

Based on the study, a picture of reattachment emerges, which is represented in Fig. 10. During deep dynamic stall of rounded leading-edge airfoils, the separated shear layer always appears to emanate from around the leading edge. However, the separation point cannot be precisely determined. As the airfoil angle of attack decreases, the shear layer starts moving toward the airfoil upper surface, without any significant reattachment until the static stall angle is approached. Reattachment begins near the static stall angle; subsequent flow development around the leading edge causes the suction pressure to increase sharply. The adverse pressure gradient following the peak suction causes the boundary layer to separate slightly downstream of the suction peak, and the separated shear layer has its origin now at this point of separation. There is a moderate angle of attack range in which the flow remains partly separated. The shear layer attaches to the surface forming a bubble only when the angle of attack falls below the static stall angle ($\simeq$ 12 deg), but it once again separates further downstream, depending on the local flow conditions. As the reattachment region proceeds toward the trailing edge, the suction pressure continues to increase with the bubble still present. Eventually, when the flow completely attaches itself over the airfoil, and the angle of attack falls to about 5 deg, the bubble disappears, and the pressures near the leading edge start to decrease. Contrary to steady flow, where the suction pressure decreases as the angle of airfoil is lowered, under dynamic conditions, there appears to be an interaction between the mechanisms of reattachment and flow development due to low positive angle of attack. During the reattachment process, the suction pressure continues to increase until reattachment is complete. Beyond this the pressure decrease is due

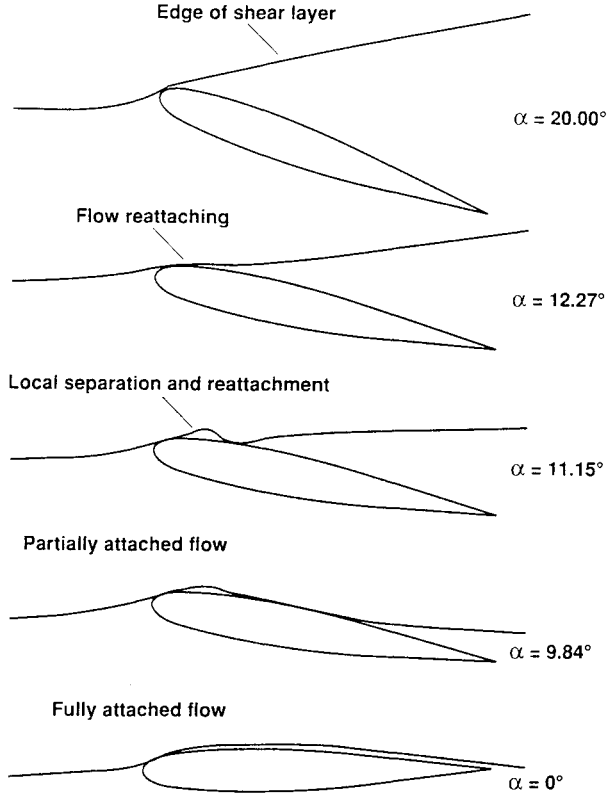

Fig. 10 Schematic of the reattachment process.

to the decrease in angle of attack only. If a mechanism is created for the reattachment to occur earlier, it is possible to reduce the hysteresis loop, thus increasing the usable lift in the cycle. Though this study has shed some light on the physics of the reattachment process, more studies are required to identify the effects of other parameters, such as airfoil geometry, on the reattachment process.

IV. Conclusions

A detailed study of the reattachment process of dynamic stall flow over an oscillating airfoil has been carried out using three different optical techniques. The major conclusions from the study are the following:

1) Reattachment of the dynamic stall flow is a continuous process, unlike that in a steady flow.

2) The process includes development of larger than freestream velocities near the airfoil surface as the process advances over it. Velocity distributions show considerable hysteresis effects.

3) Reattachment begins at or near the static stall angle even in unsteady flow. As the flow begins to reattach, the suction pressure coefficient rises rapidly, but its values are different from those in the steady flow and the unsteady flow during the upstroke at the same angle of attack.

4) For the Reynolds number of the experiment, reattachment progresses through a separation bubble, which changes size during the process and disappears at a low angle of attack.

5) Good agreement was found between LDV and PDI studies, enhancing the confidence level of the measurements.

Acknowledgments

The work was supported by the Army Research Office Grant MIPR-ARO-132-90 to the Naval Postgraduate School and was monitored by T. L. Doligalski. Additional support was provided by the Air Force Office of Scientific Research (AFOSR), MIPR-91-0007, monitored by D. Fant and also by NAVAIR, monitored by T. S. Momiyama. The support provided by S. S. Davis, chief, Fluid Dynamics Research Branch, the discussions with L.W. Carr, U.S. Army Aero Flight Dynamics Directorate at FML, the software development contributions of P. J. Trosin, and the image processing help rendered by C. Boswell of Sterling Federal Systems are all gratefully acknowledged.

References

[1]Carr, L.W., "Progress in Analysis and Prediction of Dynamic Stall," *Journal of Aircraft,* Vol. 25, No. 1, 1988, pp. 6–17.

[2]McCroskey, W. J., "The Phenomenon of Dynamic Stall," NASA TM-81264, March 1981.

[3]Niven, A. J. M., Galbraith, R. A., and David, G. F. H., "Analysis of Reattachment During Ramp Down Tests," *Vertica,* Vol 13, No. 2, 1989, pp. 187–196.

[4]Chandrasekhara, M. S., and Carr, L. W., "Flow Visualization Studies of the Mach Number Effects on the Dynamic Stall of Oscillating Airfoils," *Journal of Aircraft,* Vol. 27, No. 6, 1990, pp. 516–522; also AIAA Paper 89-0023, Jan. 1989.

[5]Chandrasekhara, M. S., and Ahmed, S., "Laser Velocimetry Measurements of Oscillating Airfoil Dynamic Stall Flow Field," AIAA Paper 91-1799, June 1991.

[6]Carr, L. W., Chandrasekhara, M. S., Ahmed, S., and Brock, N. J., "A Study of Dynamic Stall Using Real Time Interferometry," AIAA Paper 91-0007, Jan. 1991.

[7]Carr, L. W., Chandrasekhara, M. S., and Brock, N. J., "A Quantitative Visual Study of Unsteady Compressible Flow on an Oscillating Airfoil," AIAA Paper 91-1683, June 1991.

[8]Carr, L. W., and Chandrasekhara, M. S., "Design and Development of a Compressible Dynamic Stall Facility," *Journal of Aircraft,* Vol. 29, No. 3, 1992, pp. 314–318.

[9]Brock, N. J., Chandrasekhara, M. S., and Carr, L.W., "A Real Time Interferometry System for Unsteady Flow Measurements," *ICIASF'91 RECORD,* IEEE Publication 91CH3028-8, New York, Oct. 1991, pp. 423–430.

[10]Goldstein, R. J., "Optical Systems for Flow Measurement: Shadowgraph, Schlieren, and Interferometric Techniques," *Fluid Mechanics Measurements,* Hemisphere, New York, 1985, pp. 377–422.

[11]Tani, I., "Low Speed Flows Involving Bubble Separations," *Progress in Aeronautical Sciences,* No. 5, 1964, pp. 70–103.